ACCOUNTS of chemical research

Article

pubs.acs.org/accounts

Spin-Vibronic Quantum Dynamics for Ultrafast Excited-State Processes

Published as part of the Accounts of Chemical Research special issue "Ultrafast Excited-State Processes in Inorganic Systems".

Julien Eng, Christophe Gourlaouen, Etienne Gindensperger,* and Chantal Daniel*

Laboratoire de Chimie Quantique, Institut de Chimie UMR-7177, Université de Strasbourg−CNRS, 1 Rue Blaise Pascal BP 296/R8, F-67008 Strasbourg, France

CONSPECTUS: Ultrafast intersystem crossing (ISC) processes coupled to nuclear relaxation and solvation dynamics play a central role in the photophysics and photochemistry of a wide range of transition metal complexes. These phenomena occurring within a few hundred femtoseconds are investigated experimentally by ultrafast picosecond and femtosecond transient absorption or luminescence spectroscopies, and optical laser pump−X-ray probe techniques using picosecond and femtosecond X-ray pulses. The interpretation of ultrafast structural changes, time-resolved spectra, quantum yields, and time scales of elementary processes or transient lifetimes needs robust theoretical tools combining state-of-the-art quantum chemistry and developments in quantum dynamics for solving the electronic and nuclear problems. Multimode molecular dynamics beyond the Born−Oppenheimer approximation has been successfully applied to many small polyatomic systems. Its application to large molecules containing a transition metal atom is still a challenge because of the nuclear dimensionality of the problem, the high density of electronic excited states, and the spin−orbit coupling effects.

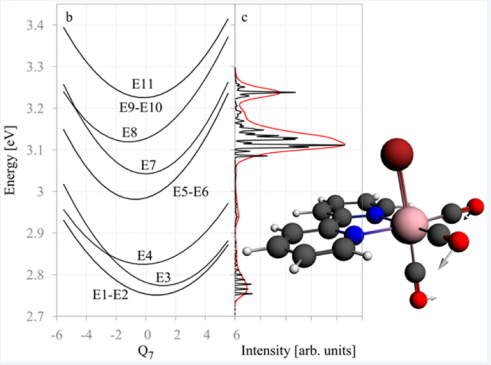

Rhenium(I) α-diimine carbonyl complexes, $[Re(L)(CO)_3(N,N)]^{n+}$ are thermally and photochemically robust and highly flexible synthetically. Structural variations of the N,N and L ligands affect the spectroscopy, the photophysics, and the photochemistry of these chromophores easily incorporated into a complex environment. Visible light absorption opens the route to a wide range of applications such as sensors, probes, or emissive labels for imaging biomolecules. Halide complexes $[Re(X)(CO)_3(bpy)]$ (X = Cl, Br, or I; bpy = 2,2′-bipyridine) exhibit complex electronic structure and large spin−orbit effects that do not correlate with the heavy atom effects. Indeed, the ^{1}MLCT → ^{3}MLCT intersystem crossing (ISC) kinetics is slower than in $[Ru(bpy)_3]^{2+}$ or $[Fe(bpy)_3]^{2+}$ despite the presence of a third-row transition metal. Counterintuitively, singlet excited-state lifetime increases on going from Cl (85 fs) to Br (128 fs) and to I (152 fs). Moreover, correlation between the Re−X stretching mode and the rate of ISC is observed.

In this Account, we emphasize on the role of spin-vibronic coupling on the mechanism of ultrafast ISC put in evidence in $[Re(Br)(CO)_3(bpy)]$. For this purpose, we have developed a model Hamiltonian for solving an 11 electronic excited states multimode problem including vibronic and SO coupling within the linear vibronic coupling (LVC) approximation and the assumption of harmonic potentials. The presence of a central metal atom coupled to rigid ligands, such as α-diimine, ensures nuclear motion of small amplitudes and *a priori* justifies the use of the LVC model. The simulation of the ultrafast dynamics by wavepacket propagations using the multiconfiguration time-dependent Hartree (MCTDH) method is based on density functional theory (DFT), and its time-dependent extension to excited states (TD-DFT) electronic structure data. We believe that the interplay between time-resolved experiments and these pioneering simulations covering the first picoseconds and including spin-vibronic coupling will promote a number of quantum dynamical studies that will contribute to a better understanding of ultrafast processes in a wide range of organic and inorganic chromophores easily incorporated in biosystems or supramolecular devices for specific functions.

1. INTRODUCTION

Ultrafast excited state processes play a central role in the photophysics and photochemistry of transition metal complexes.[1−7] Understanding and controlling the decay pathways via the low-lying singlet and triplet states manifold within the first 100 ps is key to their resourceful applications in photonics. Most of the time very short-lived metal-to-ligand-charge-transfer (MLCT) states control the kinetics of singlet−singlet and triplet−triplet internal conversion (IC) and singlet−triplet

Received: October 4, 2014
Published: February 3, 2015

DOI: 10.1021/ar500369r
Acc. Chem. Res. 2015, 48, 809−817

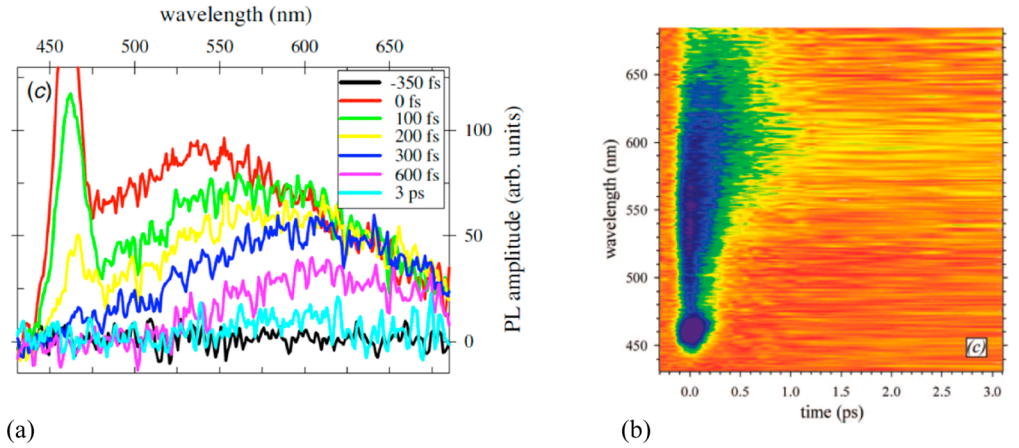

Figure 1. (a) Luminescence spectrum of [Re(Br)(CO)$_3$bpy] in CH_3CN measured at selected time delays after 400 nm excitation. (b) Two-dimensional plot of time-resolved luminescence spectrum of [Re(Br)(CO)$_3$bpy] in CH_3CN measured after 400 nm excitation. Adapted with permission from ref 18. Copyright 2008 American Chemical Society.

intersystem crossing (ISC) occurring immediately after light absorption within a few tens of femtseconds to a few tens of picoseconds.[8] Solvation dynamics and presence of low-lying metal-centered (MC) or intraligand (IL) charge transfer states may take part in the complicated mechanism of deactivation.[9−14]

Ultrafast picosecond and femtosecond transient absorption or luminescence spectroscopies and optical laser pump-X-ray probe techniques using picosecond and femtosecond X-ray pulses are the experiments of choice for deciphering the molecular electronic and conformational changes in real time.[15−18] Interpretation of time-resolved spectra and data from these sophisticated techniques needs solid developments in theory. Quantum chemistry has to handle high densities of various close-lying electronic excited states in a limited domain of energy (within 1.5 eV or 12 000 cm^{-1}) including relativistic effects, especially spin−orbit coupling (SOC).[19−21] Quantum dynamics has to treat dynamical processes that are not confined to a single electronic potential energy surface and that violate the Born−Oppenheimer separation of electronic and nuclear motions, taking into account nonadiabatic coupling between two or more electronic states via several vibrational modes.[22] Various methods of electronic structure theory are able to calculate electronic excited states and potential energy curves in transition metal complexes. Time-dependent density functional theory (TD-DFT)[23−25] and complete-active-space self-consistent-field (CASSCF)[26] combined with CAS-perturbation second order (CASPT2)[27,28] are among the most popular methods for computing electronic excited states and associated nuclear forces in this class of molecules with reasonable accuracy. The bottleneck is the computation of accurate multidimensional potential energy surfaces, seat of the ultrafast dynamics observed in time-resolved experiments. In order to bypass these difficulties two strategies can be considered: (i) *ab initio* molecular dynamics where efficient electronic structure methods are coupled to classical trajectory-based approaches;[29] (ii) quantum dynamics where both electronic and nuclear wave functions are treated exactly within a given level of approximation.[22,30−32] Molecular dynamics, usually coupled to DFT methods and extended recently to the nonadiabatic regime,[29,33,34] is adapted to large systems involving a restricted number of active electronic excited states in the dynamical process. The applicability of the full quantum approach is limited by the nuclear dimensionality and requires very robust electronic structure methods for excited states.[35] An additional difficulty in transition metal complexes is the simultaneous treatment of nonadiabatic and spin−orbit coupling.[36−39]

A recent promising approach, applied[5] to the spin crossover complex $[Fe(bpy)_3]^{2+}$,[5] has been developed by C. M. Marian et al.[40,41] This method is based on time-dependent calculations of ISC rates in the multimode harmonic oscillator and Condon approximations and beyond, where the electronic spin−orbit matrix elements depend linearly on the nuclear coordinates within a spin-vibronic coupling scheme. The ISC rate can be decomposed into three contributions, namely, direct, mixed direct-vibronic, and vibronic.

The first simulation based on TD-DFT energies and forces (gradient and Hessian) computed on-the-fly and introducing both vibronic and SO coupling effects into the Tully's trajectory surface hopping algorithm has been able to reproduce semiquantitatively the ultrafast relaxation of the photoexcited ^{1}MLCT state of $[Ru(bpy)_3]^{2+}$ (bpy = 2,2′-bipyridine) followed by ISC to the lowest ^{3}MLCT state.[42]

Combined effects of Jahn−Teller (JT) and SOC on the adiabatic PES and electronic spectra of a series of first-row transition metal halides MF_3 (M = Mn, Co, Ti, Cr, and Ni) have been recently investigated from first-principles methods based on the derivation of a Hamiltonian expanded up to linear, quadratic, and higher order in normal mode displacements active for JT distorsions and including SO up to first order in these modes.[36,43] This original work has put in evidence SO induced JT distorsions not detectable by the standard model in which SOC is considered as a static property independent of the nuclear motion.

These pioneering dynamical simulations performed on transition metal complexes are far from being routine and need specific developments to be applicable to a wide range of systems and ultrafast phenomena circumscribed by spin-vibronic coupling.

In order to decipher the photophysics of rhenium(I) tricarbonyl complexes, [Re(X)(CO)$_3$bpy)] (X = Cl, Br, or I; bpy = 2,2′-bipyridine), recently investigated by means of ultrafast luminescence spectroscopy,[18] we have developed an effective matrix Hamiltonian for solving an 11 electronic excited states multimode problem including vibronic and SO coupling within the simplified linear vibronic coupling (LVC) model and

DOI: 10.1021/ar500369r
Acc. Chem. Res. 2015, 48, 809−817

Scheme 1. Change of Electronic Density Induced by Excitation of the Electronic Ground State of $[Re(Br)(CO)_3(bpy)]$ in the Lowest Singlet (S1 and S2) and Triplet (T1, T2, and T3) Excited States[a]

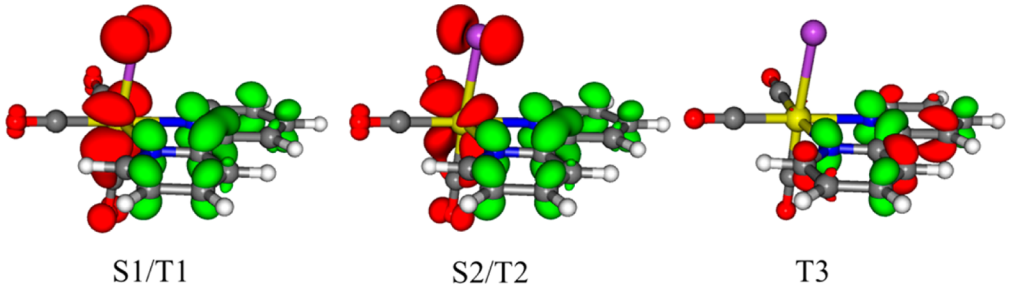

[a]In red, loss; in green, gain.

the assumption of harmonic diabatic potentials.[22,30] Our aim is to shed light on the following fundamental questions: (i) Why does the singlet excited-state lifetime counterintuitively increase on going from chloride (85 fs) to bromide (128 fs) and iodide (152 fs), whereas SOC between the singlet and triplet states increases within the series? (ii) How can we explain the correlation observed between the ISC kinetics and vibrational period of the Re−X stretching mode in similar complexes? (iii) How can we interpret the time-resolved luminescence spectra observed in CH_3CN after absorption at 400 nm, namely, a band between 500 and 550 nm (τ_1 80−150 fs), an intermediate band at about 600 nm (τ_2 0.3−1.2 ps), and a long-lived signal at 600−610 nm ($\tau_3 \approx 10$ μs) (Figure 1)?

2. QUANTUM CHEMISTRY OF [Re(Br)(CO)$_3$bpy)]

The details about the electronic properties of the series $[Re(X)(CO)_3bpy)]$ (X = Cl, Br, I) can be found in recent articles by Záliš et al. and by us.[18,19,44−46] By combining spectroscopic measurements and CASSCF/MS-CASPT2 and TD-DFT calculations, we have shown that whereas both spin-free and spin−orbit quantum chemical calculations simulate UV−vis electronic spectra of $[Re(X)(CO)_3bpy)]$ (X = Cl, Br, or I) complexes in a reasonable agreement with experiment, they give a very different interpretation of the absorption bands and only the SO treatment can account for the observed spectral features.[44,46] Going further we computed the spin−orbit coupled TD-DFT potential energy curves as a function of the Re−X bond elongation, as well as of the Re−X bond stretching modes, for the electronic ground state and the lowest excited states of $[Re(X)(CO)_3(bpy)]$ (X = Cl, Br, or I) taking into account solvent effects.[19,46] When SOC is activated the five lowest electronic excited states, S1, S2, T1, T2, and T3, the electronic densities of which are depicted in Scheme 1 for $[Re(Br)(CO)_3(bpy)]$, generate 11 "spin−orbit" states of mixed metal-to-ligand-charge-transfer MLCT/halide-LCT character within 0.5 eV, see Scheme 2 and Figure 2 further below.

According to the spin C_s double group symmetry rules, T1 and T3 (^{3}A″) states generate two A′ and one A″ "spin−orbit" states, T2 (^{3}A′) generates two A″ and one A′ "spin−orbit" states, S1 (^{1}A″) generates one A″ state, and S2 (^{1}A′) generates one A′ state. The two lowest A′ and A″ states, E1 and E2, are degenerate and composed of 66%T1 and 30%T2, whereas the next states, E3 (A′) and E4 (A″), are composed of 85%T1/11% S2 and 44%S1/50%T2, respectively. E5 and E6 of A″ and A′ symmetry, respectively, and counterparts of E1, E2, are degenerate, and are composed of 67%T2 and 31%T1. E7 (A″) is the counterpart of E4 and is composed of 51%T2 and 48%S1. The upper state E8 of symmetry A′ is characterized by

Scheme 2. Representation of the Interplay of Intersystem Crossing (ISC) and Internal Conversion (IC) Mechanisms within the Singlet and Triplet Manifolds of $[Re(Br)(CO)_3(bpy)]$

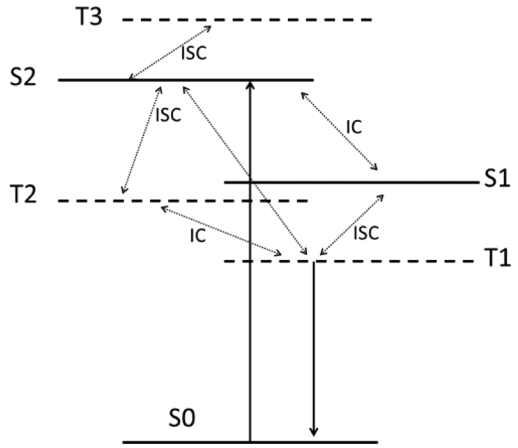

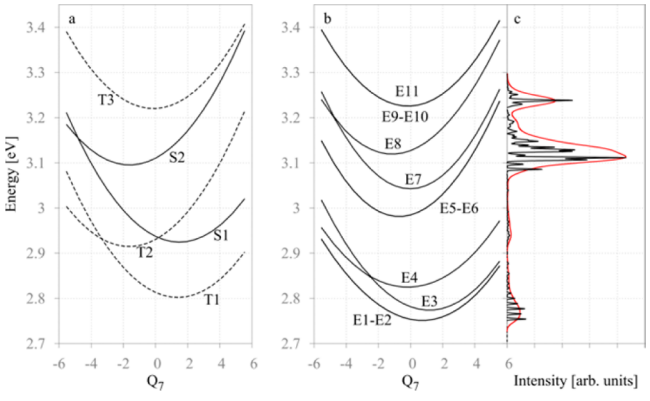

Figure 2. (a) Diabatic potential energy curves along Q_7. Each triplet state is triply degenerate. (b) Corresponding adiabatic potential energy curves. (c) Calculated absorption spectrum with its envelope after excitation of the S2 state. S2 (E8) is the strongly absorbing A′ state.

an oscillator strength of 0.036 and is described by 70% of the S2 (^{1}A′) absorbing state, with a contribution of 10% from T3 (^{3}A″). The E9 (A″) and E10 (A′) remain of quasi-pure triplet character (95% T3), while E11 (A′) is the counterpart of E8 with 82%T3/16%S2.

From the lowest electronic excited state optimized geometries, we can extract seven minima after perturbative SOC treatment of each state in its optimized structure.[46] From these electronic structure calculations performed in CH_3CN, we have

DOI: 10.1021/ar500369r
Acc. Chem. Res. 2015, 48, 809−817

proposed the following qualitative mechanism for the deactivation pathway of [Re(Br)(CO)$_3$(bpy)]. At very short time-scale, the activation of the Re−Br normal mode in S2, strongly correlated to the τ_1 time-scale (128 fs), initiates the decay to S2 minimum and S1/T2. The four upper "spin-orbit" states of A′ and A″ symmetries are potentially luminescent in the 510−550 nm energy domain. As soon as S1 and T1 are populated within the τ_2 time-scale (470 fs) correlated to SOC, the two "spin-orbit" states A″ and A′ calculated at 572 and 582 nm can luminesce as well at about 580 nm. The only purely phosphorescent state is the "spin-orbit" state calculated at 610 nm that contributes to the long time-scale decay observed at 600−620 nm. Exploratory wavepacket propagations on spin−orbit coupled potential energy curves has been able to simulate partly the ultrafast ISC process observed experimentally via the A′ channels pointing to the importance of vibronic spin−orbit coupling in transition metal complexes. This study[46] proposed a new picture for a comprehensive understanding of ultrafast ISC processes in transition metal complexes. However, the one-dimensional "spin-orbit" potential energy curves give a crude approximation of the complicated set of potential energy surfaces underlying the ultrafast decay mechanism after irradiation to S2. Indeed conical intersections may be present in the adiabatic multidimensional PES and vibronic coupling should play a role in the decay mechanism.

In this Account, we report the first quantum dynamical simulation of ultrafast nonradiative decay in the prototype transition metal complex [Re(Br)(CO)$_3$(bpy)], involving the five low-lying singlet and triplet excited states. The multimode dynamics of these five low-lying excited states are investigated on the basis of DFT and TD-DFT electronic structure data taking into account SOC in a spin-vibronic coupling model.

3. THEORETICAL BACKGROUND AND METHODOLOGY

3.1. The Model Hamiltonian

Five low-lying "spin-free" singlet and triplet excited states of [Re(Br)(CO)$_3$bpy] are in the energy domain close to the experimental 400 nm (3.10 eV) excitation energy, namely, S2 (a^1A') calculated at 3.13 eV (399 nm) with an oscillator strength $f = 5.1 \times 10^{-2}$, S1 (a^1A'') calculated at 2.96 eV ($f = 0.17 \times 10^{-2}$), and the lowest triplets T3 (b^3A''), T2 (a^3A'), and T1 (a^3A'') calculated at 3.22, 2.93, and 2.84 eV, respectively.[44,46]

In the Pauli approximation, the electronic Hamiltonian $\mathbf{H}^{el}$ is expressed as the sum of the nonrelativistic (electrostatic), $\mathbf{H}^{es}$, and the "spin−orbit", $\mathbf{H}^{SO}$, Hamiltonians:

$$\mathbf{H}^{el} = \mathbf{H}^{es} + \mathbf{H}^{SO}$$

The $\mathbf{H}^{es}$ Hamiltonian contains the energy of the "spin-free" states as diagonal elements (triply degenerate for the triplets), while the $\mathbf{H}^{SO}$ Hamiltonian is comprised of the SOC off-diagonal terms. If one diagonalizes the $\mathbf{H}^{el}$ Hamiltonian, one recovers the energy of the "spin-orbit" states.

The 11 × 11 (2 singlets + 3 × 3 triplet components) total Hamiltonian is expressed as

$$\mathbf{H} = T_N\mathbf{1} + \mathbf{H}^{el}$$

where T_N is the kinetic energy of the nuclei, $\mathbf{1}$ is the identity matrix, and $\mathbf{H}^{el}$ depends on the nuclear coordinates. Within the vibronic coupling approach,[22] the effective matrix Hamiltonian reads

$$\mathbf{H} = (T_N + V_0)\mathbf{1} + \mathbf{W}$$

where V_0 is the ground state potential energy surface, here taken to be harmonic with vibrational frequencies ω_i along dimensionless normal coordinates Q_i determined from the electronic structure calculations at the ground state equilibrium geometry (Franck−Condon point, FC). The matrix Hamiltonian $\mathbf{W}$ contains the spin−orbit coupling terms plus the vibronic coupling terms. The vibronic coupling terms are obtained from a Taylor expansion of the "spin-free" potential energy surfaces up to first order around FC.[22]

The multistate vibronic interactions within the set of the five "spin-free" electronic excited states (n = 1−5) are deduced from the diabatic electronic representation including all pertinent coupling terms, namely, the intrastate κ^n and interstate $\lambda^{n,m}$ vibronic coupling constants between the n and m electronic states and the (complex-valued) $\eta^{n,m}$ SOC constants deduced from the electronic structure calculations. Within the LVC approach, the nonvanishing intrastate κ^n and interstate $\lambda^{n,m}$ coupling constants are those for which the product of the irreducible representations of states n and m and of the nuclear normal mode coordinate Q_i contains the totally symmetric representation Γ_A (A′ in C_s):

$$\Gamma_n \otimes \Gamma_{Q_i} \otimes \Gamma_m \subset \Gamma_A$$

In the C_s symmetry point group, only vibrational modes of a′ symmetry can have nonvanishing κ^n coupling constant while only a″ vibrational modes will contribute to the off-diagonal coupling $\lambda^{n,m}$. The coupling constants can be obtained from the following expressions[22] evaluated at $Q_i = 0$:

$$\kappa_i^n = \frac{\partial V_n}{\partial Q_i}$$

$$\lambda_i^{n,m} = \left(\frac{1}{8}\frac{\partial^2}{\partial Q_i^2}(|V_m - V_n|^2)\right)^{1/2}$$

where V_n is the adiabatic potential energy surface of the "spin-free" state n. That is, only the gradients and the Hessians at FC are needed within this model. The SOC will generally also depend on the nuclear displacements. However, they are kept constant here, that is, the FC values are used. With those ingredients, the unitary potential energy matrix, $\mathbf{W}$, is

$$\mathbf{W} = \begin{pmatrix} \mathbf{W}^{T1,T1} & \mathbf{W}^{T1,T2} & 0 & \mathbf{W}^{T1,S2} & 0 \\ \mathbf{W}^{*T1,T2} & \mathbf{W}^{T2,T2} & \mathbf{W}^{T2,S1} & 0 & \mathbf{W}^{T2,T3} \\ 0 & \mathbf{W}^{*T2,S1} & \mathbf{W}^{S1,S1} & \mathbf{W}^{S1,S2} & 0 \\ \mathbf{W}^{*T1,S2} & 0 & \mathbf{W}^{*S1,S2} & \mathbf{W}^{S2,S2} & \mathbf{W}^{S2,T3} \\ 0 & \mathbf{W}^{*T2,T3} & 0 & \mathbf{W}^{*S2,T3} & \mathbf{W}^{T3,T3} \end{pmatrix}$$

where the asterisk stands for the conjugate transpose and with the submatrices

DOI: 10.1021/ar500369r
Acc. Chem. Res. 2015, 48, 809−817

Table 1. List of the Parameters Entering the Model Hamiltonian[a]

mode	ω	κ				
		S1	S2	T1	T2	T3
7 (a′)	0.0116	−0.0172	0.0187	−0.0161	0.0190	0.0015
11 (a′)	0.0188	0.0090	0.0091	0.0002	−0.0006	0.0056
13 (a′)	0.0229	−0.0289	−0.0271	−0.0261	−0.0322	0.0133
30 (a′)	0.0792	−0.0187	0.0404	−0.0196	0.0433	0.0033

mode	ω	λ^{S1S2}	λ^{T1T2}
8 (a″)	0.0118	0.0114	0.0086
23 (a″)	0.0601	0.0237	0.0190

State	E		η	
state	calcd	adjd		
S1 (A″)	2.96	2.94	S1T2	0.0769 + 0.0186i
S2 (A′)	3.13	3.11	S2T1	−0.0719 − 0.0196i
T1 (A″)	2.84	2.81	S2T3	0.0274 + 0.0056i
T2 (A′)	2.93	2.93	T1T2	0.0719 + 0.0177i
T3 (A″)	3.22	3.22	T2T3	−0.0270 + 0.0046i

[a]Values are given in eV. E is the vertical excitation energy. Calcd indicates the calculated values from ref 46. Adjd indicates the adjusted values used in this work.

$$\mathbf{W}^{n,n} = E_n + \sum_{i\in a'} \kappa_i^{\,n} Q_i; \quad \mathbf{W}^{S1,S2} = \sum_{j\in a''} \lambda_j^{S1,S2} Q_j;$$

$$\mathbf{W}^{S2,T3} = (\eta^*_{S2T3};\ 0;\ \eta_{S2T3});$$

$$\mathbf{W}^{Tn,Sm} = \begin{pmatrix} \eta_{SmTn} \\ 0 \\ \eta^*_{SmTn} \end{pmatrix},\ n, m = 1, 2;$$

$$\mathbf{W}^{T1,T2} = \begin{pmatrix} \sum_{j\in a''} \lambda_j^{T1,T2} Q_j & \eta_{T1T2} & 0 \\ -\eta^*_{T1T2} & \sum_{j\in a''} \lambda_j^{T1,T2} Q_j & \eta_{T1T2} \\ 0 & -\eta^*_{T1T2} & \sum_{j\in a''} \lambda_j^{T1,T2} Q_j \end{pmatrix};$$

$$\mathbf{W}^{T2,T3} = \begin{pmatrix} 0 & \eta_{T2T3} & 0 \\ -\eta^*_{T2T3} & 0 & \eta_{T2T3} \\ 0 & -\eta^*_{T2T3} & 0 \end{pmatrix}$$

In each submatrix, the triplet components are ordered by ascending m_s values. E_n is the vertical excitation energy of the "spin-free" state n. Note that some of the zeros in $\mathbf{W}$ come from (C_s) symmetry constraint and others from the fact that the corresponding computed coupling constants have very small values and are thus disregarded in the present study. In addition, coupling to higher lying states, in particular S3 and T4, is not included in the study along with the T2/T3 vibronic coupling neglected here (see $\mathbf{W}^{T2,T3}$ above). Note that T3 is of IL_{bpy} nature, in contrast to all other states of MLCT/XLCT nature (see Scheme 1), and is included here mainly because it contributes to the "spin-orbit" absorbing state E8.

The proposed model Hamiltonian is probably the simplest one that can be constructed with only relatively few electronic structure data (all obtained at FC), but still treating explicitly all triplet components and thus accounting for the triplet's multiplicity.

3.2. Electronic Structure Data

The detailed data of the electronic structure calculations are reported elsewhere.[46] All the data used in the present work have been determined by means of DFT and TD-DFT methods including polarized continuum model (PCM)[47,48] solvent corrections and using the functional B3LYP[49] with all electrons and triple-ζ basis sets.[50] The scalar relativistic effects have been taken into account within the zero-order regular approximation (ZORA).[51] The SOC effects have been introduced according to a simplified relativistic perturbative TD-DFT formalism.[52] The TD-DFT calculations have been validated by accurate CASSCF/multistate-CASPT2 methods.[44]

3.3. Wavepacket Propagation by MCTDH

The time-dependent Schrödinger equation for the nuclei is solved by employing the MCTDH method.[53−55] Here, the multiconfiguration nuclear wave function is expressed as a Hartree product of time-dependent basis functions, known as single-particle functions. The wavepacket ansatz adapted to the present nonadiabatic problem corresponds to the multiset formulation.[54] The Heidelberg MCTDH Package[56] is used (version 8.4.9).

4. RESULTS

4.1. Vibrational Modes Selection

The gradients and Hessians of the energy have been computed analytically and numerically, respectively, at the FC geometry, to evaluate the κ^n and $\lambda^{n,m}$ coupling constants. The [Re(Br)-$(CO)_3$bpy]$^+$ complex possesses 78 internal degrees of freedom, among which 41 are of a′ symmetry and 37 are of a″ symmetry. All of the computed κ^n and $\lambda^{n,m}$ values are small, order of 10^{-2} to 10^{-3} eV. This is not surprising because the molecule is quite rigid, and moreover S1, S2, T1, and T2 are characterized by the same electronic structure. Based on the κ^n and $\lambda^{n,m}$ values, only six nuclear degrees of freedom, four a′ and two a″ modes, are included in the present dynamical study. The corresponding values entering the model Hamiltonian are provided in Table 1. The four a′ modes are divided in two groups. The first one includes the two vibrational modes, ν_{11} and ν_{13}, that involve stretching of the Re−Br bond; the modes are labeled according to increasing frequency. They are calculated to have frequencies

DOI: 10.1021/ar500369r
Acc. Chem. Res. 2015, 48, 809−817

of ω_{11} = 152 cm^{-1} and ω_{13} = 185 cm^{-1}. They both exhibit contributions of motion of the bpy moiety. The largest Re−Br stretch contribution is by far for the ν_{11} mode; it is relatively small for ν_{13}. These modes are included in the present treatment because of the experimentally found correlation between excited state lifetimes and the Re−Br vibrational frequency.[18] In fact, these two modes do have κ^n of the same sign for S1, T1, S2, and T2, meaning that they shift all those electronic states toward the same direction. This common sign is again not surprising, since we are dealing with charge transfer to the bpy (except T3): they all react the same if we stretch the Re−Br bond. However, the strongest nonadiabatic effect is obtained when the κ^n have opposite signs and largest absolute values. This is achieved here for two other a′ modes, ν_7 and ν_{30} of frequency ω_7 = 94 cm^{-1} and ω_{30} = 638 cm^{-1}. These modes both involve motion of the carbonyl groups. These motions of the CO groups have a different impact on the d_{xy} (involved in S0−S2/T2 transitions) and d_{yz} (involved in S0−S1/T1 transitions) orbitals of the metal, leading to the opposite sign in the coupling constants.

Among the a″ modes, a large number of them do not have a $\lambda^{n,m}$ coupling constant that leads to a coupling (the computed values are purely imaginary, meaning that S1/S2 on the one hand and T1/T2 on the other hand do not repel each other.) Interestingly, some modes are found at this level of description that couple at the same time S1 with S2 and T1 with T2. Large coupling constants are found for ν_8 (ω_8 = 95 cm^{-1}) and ν_{23} (ω_{23} = 485 cm^{-1}). These are both modes that involve symmetry breaking motions of the carbonyl groups. They are the nontotally symmetric companions of the totally symmetric ν_7 and ν_{30}.

These six modes are included for the study of the quantum dynamics of the [Re(Br)(CO)$_3$bpy] complex to gain access to the absorption spectrum and short-time electronic population dynamics.

4.2. Potential Energy Surfaces and Absorption Spectrum

The diabatic potential energy surfaces are used for the quantum dynamics. They are shown in Figure 2a along a single vibrational mode, Q_7. In Figure 2b, the 11 corresponding adiabatic potential energy curves are provided. These curves are obtained from the diagonalization of the diabatic Hamiltonian matrix. Figure 2c displays the associated absorption spectrum that is evaluated as the Fourier transform of the autocorrelation function obtained with MCTDH.[54] A total propagation time of 1 ps is used, after excitation of the S2 state.

In our calculations, we have used slightly adjusted vertical transition energies for S1, S2, and T1, see Table 1, variation of 0.03 eV at most. These values are adjusted in order to recover the computed transition energies of the "spin-orbit" states at FC. Indeed the state T4, excluded from the present study, interacts by spin−orbit with these three states. Its static effect is thus taken into account indirectly when using the adjusted values.

The diabatic potential energy curves (Figure 2a) show the intersections between S1/S2 and T1/T2. The vibronic off-diagonal term allows population transfer between these states. In contrast to the regular vibronic coupling Hamiltonian without SOC, the adiabatic energies at FC are vertically shifted by constant values here, values directly related to the SOC constants. The E1/E2 and E9/E10 states remain degenerate, and S2 contributes mainly to E8 (70%) at 3.13 eV and slightly to E11 (16%) and E3 (10%). See section 2 and ref. [46] for the description of the spin-adiabatic states.

The spectra computed after transition to the diabatic S2 state are characterized by three bands, corresponding to E1−E3 at ∼2.76 eV, E7/E8 at ∼3.10 eV, and E9−E11 at ∼3.22 eV. E4−E6 do not contribute to the absorption. Regarding the E7/E8 band, one can see that absorption occurs below the minimum of E8(A′) along Q_7. Indeed, the global minimum within our six dimensional potential is lower in energy. Furthermore, some intensity is borrowed from the A″ E7 state by vibronic coupling. The vibrational progression, which can be seen in the E1−E3 band, corresponds to the ν_7 low frequency. In the E7/E8 band, it is more intricate; ν_{11} and ν_{13} modes do contribute to the absorption band.

4.3. Excited-State Population Dynamics

The evolution of the diabatic electronic populations as a function of time is shown in Figure 3 after initial excitation of S2. For convenience, the populations of the individual triplet components are summed over. The S2 population decreases very rapidly, within 10−20 fs, to reach a value of ∼50%. This is purely due to the SOC to T1 and T3. The fast oscillations in T1 and T3 are directly related to the strength of the SOC. After this initial decay, the S2 population further decays until ∼320 fs, while the population of T1 remains rather constant. Indeed, this S2 decay is due to SOC to T2 (A′ component) in addition to vibronic coupling to S1. S1 in turn populates T2 (A″ components) due to strong S1/T2 SOC. The population of the T3 state, which lies above S2, decreases slowly after 20 fs. Around 350 fs, we do see a recurrence in the T1 (and S2) population. In fact, this corresponds to the period associated with ν_7 and twice that of ν_{13}. That is, after 350 fs our results can no longer be exploited: additional nuclear degrees of freedom would have killed those recurrences. This also goes in line with the small value of vibronic coupling with respect to the SOC (see Table 1). This strongly suggests that the population dynamics at longer time is not governed by some particular vibrational modes but rather by collective effects.

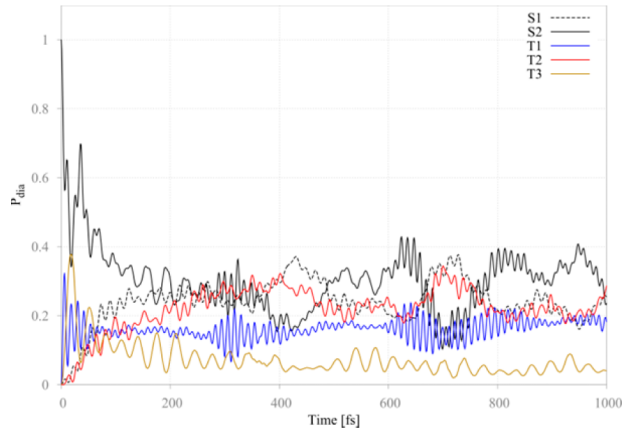

Figure 3. Diabatic electronic populations as a function of time. The triplet components are summed over. The S2 population drops very quickly due to SOC and then evolves further due to vibronic coupling.

It is also very instructive to analyze the evolution of the adiabatic populations (Figure 4). These are calculated from the diabatic ones with MCTDH by using the Monte Carlo integration scheme with default parameters.[56] At time zero, E8, E3, and E11, all of A′ symmetry, are initially populated

DOI: 10.1021/ar500369r
Acc. Chem. Res. 2015, 48, 809−817

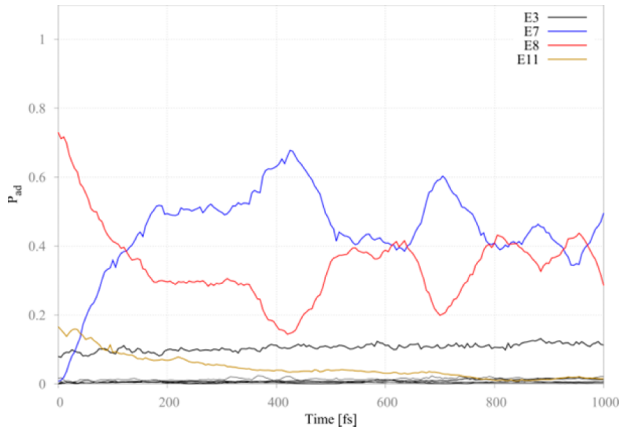

Figure 4. Adiabatic electronic populations as a function of time. The E8 (A′) population decreases to populate E7 (A″) by vibronic coupling. Only four adiatabic "spin-orbtit" states are significantly populated in the first 350 fs.

because they have contributions from the S2 state of 70%, 10%, and 16%, respectively (see section 2).[46] The first observation is that these adiabatic populations do not oscillate as the diabatic ones do. This is not surprising since the (constant) SOC acts in the adiabatic picture as diagonal contributions to the Hamiltonian: it does not induce population transfer anymore.

In Figure 4, we observe that only four "spin-orbit" states are significantly populated. In particular, we see that the population of E8 is mainly transferred to a single other "spin-orbit" state, E7 (A″). This state is composed of 51%T2 and 48%S1 and is populated because of the S1/S2 vibronic coupling and S2/T2 SOC. The E8 population drops up to 0.3 in ∼180 fs and then stays constant up to 350 fs. The E8 and E7 adiabatic population curves cross at about 130 fs. The population of E3, composed of 85% T1, remains almost constant, as the diabatic population of T1 does. In fact it increases very slowly, with a large time constant. Finally, the population of E11 (82% T3) decreases slowly to repopulate E8.

The E8 state has been calculated to emit (relaxed excited state geometry) at 505 nm, the E3 state at 600 nm, the E11 state at 490 nm, and the E7 state at 580 nm.[46] Upon absorption at 400 nm used in experiment,[18] the E8 state is populated. The nuclear relaxation within this state, together with E11, will be responsible for the ∼500 nm emission band. The population of the vibronically coupled E7 state within the first 130 fs correlates with the observed emission around 580 nm. The E3 state explains the long-lived 600−610 emission band. Of course the phosphorescent E1 and E2 states will also contribute (95% T1). They are however very weakly populated using the present model because of the very small T1/T2 vibronic coupling constant.

The time scales of the present study, for example, the ∼130−180 fs decrease (rise) time of the E8 (E7) state population, are in the same order as the τ_1 = 128 fs deduced from the time-resolved emission spectra,[18] which is satisfactory given the model used. The second measured decay time τ_2 = 470 fs cannot be studied here because of our reduced dimensionality approach, which leads to recurrences in the population dynamics. Other vibrational modes need to be included, in particular for the T1/T2 coupling, and to avoid the recurrences.

5. CONCLUSIONS

In this Account, we have shown that it is possible to construct a model Hamiltonian to study the quantum dynamics of transition metal complexes involving several electronic states and accounting for both spin−orbit and vibronic coupling. This model Hamiltonian requires limited data from electronic structure calculations. While we have applied it in its simplest form, it is possible to systematically increase its complexity to account for additional effects. The first application to the study of the ultrafast relaxation in the $[Re(Br)(CO)_3(bpy)]$ complex after excitation at 400 nm allows us to confirm that the fast decay of the initially populated electronic state is mainly due to vibronic coupling, with a time scale on the order of the experimentally found one. This study shows that, rather than important contributions of some few vibrational modes, it is collective effects that play a key role in this class of complexes. Inclusion of additional degrees of freedom and possibly higher order terms in the Hamiltonian, and comparison with the study of the $[Re(X)(CO)_3(bpy)]$, X = Cl or I, complexes will allow us to analyze in more detail the interplay between spin−orbit and vibronic coupling in transition metal complexes using a full quantum treatment.

AUTHOR INFORMATION

Corresponding Authors

*E-mail: egindensperger@unistra.fr.
*E-mail: c.daniel@unistra.fr.

Notes

The authors declare no competing financial interest.

Biographies

Julien Eng graduated in Physical Chemistry from the University of Strasbourg. Since 2012, he has been a Ph.D. student in the Laboratoire de Chimie Quantique Strasbourg. Current interests are theoretical studies of isomerization pathways in organic and inorganic systems from both the quantum chemical and quantum dynamical perspectives.

Christophe Gourlaouen received his Ph.D. (2006) from the University Pierre & Marie Curie, Paris. In 2007, he joined ICQC, Tarragona, Spain, where he performed post-doctoral research with Feliu Maseras and then moved in 2008 to the CEA. Since 2010, he has been CNRS-researcher at the Laboratoire de Chimie Quantique, Strasbourg, as Chargé de Recherche. Current interests are electronic structure in transition metal complexes, bonding in polymetallic systems, and more recently luminescent properties.

Etienne Gindensperger received his Ph.D. in 2004 from the Université Paul Sabatier, Toulouse, France. He then joined the Theoretical Chemistry group of the University of Heidelberg, Germany, as a Alexender von Humbold fellow. Since 2007, he has been CNRS-researcher at the Laboratoire de Chimie Quantique, Institut de Chimie, Université de Strasbourg. Current interests are focused on the theoretical description of ultrafast photoinduced processes in organic and inorganic systems.

Chantal Daniel received her Ph.D. in 1985 from the University of Strasbourg. She joined the group of Keiji Morokuma at IMS, Okazaki, Japan, in 1986 as JSPS fellow and then the IBM Department in Kingston, NY, USA, as postdoctoral associate of Michel Dupuis in 1988. Since 1999, she has been CNRS-researcher at the Laboratoire de Chimie Quantique as Directeur de Recherche. Current interests are excited state properties in transition metal complexes and modeling

DOI: 10.1021/ar500369r
Acc. Chem. Res. 2015, 48, 809−817

and simulation of photochemical and photophysical properties of molecules in complex environments.

■ ACKNOWLEDGMENTS

The authors thank A. Vlček Jr., M. Chergui, and A. Cannizzo for having motivated this work. The European actions COST perspect-H2O and CODEC are acknowledged. The calculations have been performed on the computer nodes of the LCQS, Strasbourg, and the High-Performance Computing center (pole HPC) at Université de Strasbourg.

■ REFERENCES

(1) Juban, E. A.; Smeigh, A. L.; Monat, J. E.; McCusker, J. K. Ultrafast dynamics of ligand-field excited states. *Coord. Chem. Rev.* **2006**, *250*, 1783−1791.

(2) McCusker, J. K. Femtosecond absorption spectroscopy of transition metal charge-transfer complexes. *Acc. Chem. Res.* **2003**, *36*, 876−887.

(3) Chergui, M. On the interplay between charge, spin and structural dynamics in transition metal complexes. *Dalton Trans.* **2012**, *41*, 13022−13029.

(4) Bräm, O.; Messina, F.; Baranoff, E.; Cannizzo, A.; Nazeeruddin, M. K.; Chergui, M. Ultrafast relaxation dynamics of osmium-polypyridine complexes in solution. *J. Phys. Chem. C* **2013**, *117*, 15958−15966.

(5) Sousa, C.; de Graaf, C.; Rudavskyi, A.; Broer, R.; Tatchen, J.; Etinski, M.; Marian, C. M. Ultrafast deactivation mechanism of the excited singlet in the light-induced spin crossover of $[Fe(2,2'\text{-bipyridine})_3]^{2+}$. *Chem.—Eur. J.* **2013**, *19*, 17541−17551.

(6) El Nahhas, A.; Consani, C.; Blanco-Rodríguez, A. B.; Lancaster, K. M.; Braem, O.; Cannizzo, A.; Towrie, M.; Clark, I. P.; Záliš, S.; Chergui, M.; Vlček, A., Jr. Ultrafast excited-state dynamics of rhenium(I) photosensitizers $[Re(Cl)(CO)_3(N,N)]$ and $[Re(\text{imidazole})(CO)_3(N,N)]^+$: Diimine effects. *Inorg. Chem.* **2011**, *50*, 2932−2943.

(7) Renske, M.; van der Veen, R. M.; Cannizzo, A.; van Mourik, F.; Vlček, A., Jr.; Chergui, M. Vibrational relaxation and intersystem crossing of binuclear metal complexes in solution. *J. Am. Chem. Soc.* **2011**, *133*, 305−315.

(8) Damrauer, N. H.; Cerullo, G.; Yeh, A.; Boussie, T. R.; Shank, C. V.; McCusker, J. K. Femtosecond dynamics of excited-state evolution in $[Ru(bpy)_3]^{2+}$. *Science* **1997**, *275*, 54−57.

(9) El Nahhas, A.; Cannizzo, A.; van Mourik, F.; Blanco-Rodríguez, A. M.; Záliš, S.; Vlček, A., Jr.; Chergui, M. Ultrafast excited-state dynamics of $[Re(L)(CO)_3(bpy)]^{n+}$ complexes: involvement of the solvent. *J. Phys. Chem. A* **2010**, *114*, 6361−6369.

(10) Kuimova, M. K.; Alsindi, W. Z.; Blake, A. J.; Davies, E. S.; Lampus, D. J.; Matousek, P.; McMaster, J.; Parker, A. W.; Towrie, M.; Sun, X.-Z.; Wilson, C.; George, M. W. Probing the solvent dependent photophysics of *fac*-$[Re(CO)_3(\text{dppz-}X_2)Cl]$ (dppz-X_2 = 11,12-X_2-dipyrido[3,2-a:2′,3′-c]phenazine); X = CH_3, H, F, Cl, CF_3). *Inorg. Chem.* **2008**, *47*, 9857−9869.

(11) Huse, N.; Kim, T. K.; Jamula, L.; McCusker, J. K.; de Groot, F. M. F.; Schoenlein, R. W. Photo-induced spin-state conversion in solvated transition metal complexes probed via time-resolved soft X-ray spectroscopy. *J. Am. Chem. Soc.* **2010**, *132*, 6809−6816.

(12) Huse, N.; Cho, H.; Hong, K.; Jamula, L.; de Groot, F. M. F.; Kim, T. K.; McCusker, J. K.; Schoenlein, R. W. Femtosecond soft X-ray spectroscopy of solvated transition-metal complexes: Deciphering the interplay of electronic and structural dynamics. *J. Phys. Chem. Lett.* **2011**, *2*, 880−884.

(13) Bressler, Ch.; Milne, C.; Pham, V.-T.; El Nahhas, A.; van der Veen, R. M.; Gawelda, W.; Johnson, S.; Beaud, P.; Grolimund, D.; Kaiser, M.; Borca, C. N.; Ingold, G.; Abela, R.; Chergui, M. Femtosecond XANES study of the light-induced spin crossover dynamics in an iron(II) complex. *Science* **2009**, *323*, 489−492.

(14) Blanco-Rodríguez, A. M.; Kvapilová, H.; Sýkora, J.; Towrie, M.; Nervi, C.; Volpi, G.; Záliš, S.; Vlček, A., Jr. Photophysics of singlet and triplet intraligand excited states in $[ReCl(CO)_3(1\text{-}(2\text{-pyridyl})\text{-imidazo-}[1,5\text{-}\alpha]\text{pyridine})]$ complexes. *J. Am. Chem. Soc.* **2014**, *136*, 5963−5973.

(15) van der Veen, R. M.; Milne, C. J.; El Nahhas, A.; Lima, F. A.; Pham, V.-T.; Best, J.; Weinstein, J. A.; Borca, C. N.; Abela, R.; Bressler, Ch.; Chergui, M. Structural determination of a photochemically active diplatinum molecule by time-resolved EXAFS spectroscopy. *Angew. Chem., Int. Ed.* **2009**, *48*, 2711−2714.

(16) Cannizzo, A.; Milne, C. J.; Consani, C.; Gawelda, W.; Bressler, Ch.; van Mourik, F.; Chergui, M. Light-induced spin crossover in Fe(II)-based complexes: The full photocycle unraveled by ultrafast optical and X-ray spectroscopies. *Coord. Chem. Rev.* **2010**, *254*, 2677−2686.

(17) Smeigh, A. L.; Creelman, M.; Mathies, R. A.; McCusker, J. K. Femtosecond time-resolved optical and Raman spectroscopy of photoinduced spin crossover: Temporal resolution of low-to-high spin optical switching. *J. Am. Chem. Soc.* **2008**, *130*, 14105−14107.

(18) Cannizzo, A.; Blanco-Rodríguez, A. M.; El Nahhas, A.; Sebera, J.; Záliš, S.; Vlček, A., Jr.; Chergui, M. Femtosecond fluorescence and intersystem crossing in rhenium(I) carbonyl-bipyridine complexes. *J. Am. Chem. Soc.* **2008**, *130*, 8967−8974.

(19) Daniel, C. Photochemistry and photophysics of transition metal complexes: Quantum chemistry. *Coord. Chem. Rev.* **2015**, *282*−*283*, 19−32.

(20) Daniel, C. Electronic spectroscopy and photoreactivity of transition metal complexes: Quantum chemistry and wave packet dynamics. In *Transition Metal and Rare Earth Compounds: Excited States, Transitions, Interactions III* Yersin, H. Ed.; Topics in Current Chemistry; Springer-Verlag: Heidelberg, 2005; Vol. *241*, pp 119−165.

(21) González, L.; Escudero, D.; Serrano-Andrés, L. Progress and challenges in the calculation of electronic excited states. *ChemPhysChem* **2012**, *13*, 28−51.

(22) Köppel, H.; Domcke, W.; Cederbaum, L. S. Multimode molecular dynamics beyond the Born-Oppenheimer approximation. *Adv. Chem. Phys.* **1984**, *57*, 59−246.

(23) Runge, E.; Gross, E. K. U. Density-functional theory for time-dependent systems. *Phys. Rev. Lett.* **1984**, *52*, 997−1000.

(24) Petersilka, M.; Gossmann, U. J.; Gross, E. K. U. Excitation energies from time-dependent density-functional theory. *Phys. Rev. Lett.* **1996**, *76*, 1212−1215.

(25) Casida, M. E.; Huix-Rotlant, M.; Johnson, M.A.; Martinez, T. J. Progress in Time-Dependent Density-Functional Theory. *Annu. Rev. Phys. Chem.* **2012**, *63*, 287−323.

(26) Roos, B. O.; Taylor, P. R.; Siegbahn, P. E. M. A complete active space SCF method (CASSCF) using a density matrix formulated super-CI approach. *Chem. Phys.* **1980**, *48*, 157−173.

(27) Andersson, K.; Malmqvist, P. -Å.; Roos, B. O.; Sadlej, A. J.; Wolinski, K. Second-order perturbation theory with a CASSCF reference function. *J. Phys. Chem.* **1990**, *94*, 5483−5488.

(28) Andersson, K.; Malmqvist, P. -Å.; Roos, B. O. Second-order perturbation theory with a complete active space self-consistent field reference function. *J. Chem. Phys.* **1992**, *96*, 1218−1226.

(29) Curchod, B. F. E.; Rothlisberger, U.; Tavernelli, I. Trajectory-based nonadiabatic dynamics with time-dependent density functional theory. *ChemPhysChem* **2013**, *14*, 1314−1340 and references therein..

(30) Köppel, H.; Domcke, W. Vibronic dynamics of polyatomic molecules. In *Encyclopedia in Computational Chemistry*; von Ragué Schleyer, P., Ed.; Wiley: New York, 1998; p 3166.

(31) Domcke, W., Yarkony, D. R., Köppel, H., Eds. *Conical Intersections - Electronic structure, Dynamics and Spectroscopy*; Advanced Series in Physical Chemistry; World Scientific; Singapore, 2004; Vol. *15*.

(32) Baer, M. *Beyond Born-Oppenheimer: Conical Intersections and Electronic Nonadiabatic Coupling Terms*; Wiley-Interscience: Hoboken, NJ, 2006.

(33) Curchod, B. F. E.; Penfold, T. J.; Rothlisberger, U.; Tavernelli, I. Nonadiabatic *ab initio* molecular dynamics using linear-response time-

DOI: 10.1021/ar500369r
Acc. Chem. Res. 2015, 48, 809−817

dependent density functional theory. *Cent. Eur. J. Phys.* **2013**, *11*, 1059−1065.
(34) de Carvalho, F. F.; Bouduban, M. E. F.; Curchod, B. F. E.; Tavernelli, I. Nonadiabatic molecular dynamics based on trajectories. *Entropy* **2014**, *16*, 62−85.
(35) Worth, G. A.; Welch, G.; Paterson, M. J. Wavepacket dynamics of $Cr(CO)_5$ after formation by photodissociation: Relaxation through an (E⊕A)⊗e Jahn-Teller conical intersection. *Mol. Phys.* **2006**, *104*, 1095−1105.
(36) Mondal, P.; Opalka, D.; Poluyanov, L. V.; Domcke, W. Jahn-Teller and spin-orbit coupling effects in transition metal trifluorides. *Chem. Phys.* **2011**, *387*, 56−65.
(37) Ando, H.; Iuchi, S.; Sato, H. Theoretical study on ultrafast intersystem crossing of chromium (III) acetylacetonate. *Chem. Phys. Lett.* **2012**, *535*, 177−181.
(38) Baková, R.; Chergui, M.; Daniel, C.; Vlček, A.; Záliš, S. Relativistic effects in spectroscopy and photophysics of heavy-metal complexes illustrated by spin−orbit calculations of [Re (imidazole)-$(CO)_3$phen)]$^+$. *Coord. Chem. Rev.* **2011**, *255*, 975−989.
(39) Heitz, M.-C.; Ribbing, C.; Daniel, C. Spin-orbit induced radiationless transitions in organometallics: Quantum simulation of the intersystem crossing processes in the photodissociation of $HCo(CO)_4$. *J. Chem. Phys.* **1997**, *106*, 1421−1428.
(40) Etinski, M.; Tatchen, J.; Marian, C. M. Time-dependent approaches for the calculation of intersystem crossing rates. *J. Chem. Phys.* **2011**, *134*, No. 154105.
(41) Etinski, M.; Rai-Constapel, V.; Marian, C. M. Time-dependent approach to spin-vibronic coupling: Implementation and assessment. *J. Chem. Phys.* **2014**, *140*, No. 114104.
(42) Tavernelli, I.; Curchod, B. F. E.; Rothlisberger, U. Nonadiabatic molecular dynamics with solvent effects: A LR-TDDFT QM/MM study of ruthenium (II) tris (bipyridine) in water. *Chem. Phys.* **2011**, *391*, 101−109.
(43) Mondal, P.; Opalka, D.; Poluyanov, L. V.; Domcke, W. *Ab initio* study of dynamical E⊗e Jahn-Teller and spin-orbit coupling effects in the transition-metal trifluorides TiF_3, CrF_3 and NiF_3. *J. Chem. Phys.* **2012**, *136*, No. 084308.
(44) Heydová, R.; Gindensperger, E.; Romano, R.; Sýkora, J.; Vlček, A., Jr.; Záliš, S.; Daniel, C. Spin−orbit treatment of UV−vis absorption spectra and photophysics of rhenium(I) carbonyl−bipyridine complexes: MS-CASPT2 and TD-DFT Analysis. *J. Phys. Chem. A* **2012**, *116*, 11319−11329.
(45) El Nahhas, A.; van der Veen, R. M.; Penfold, T. J.; Pham, V. T.; Lima, F. A.; Abela, R.; Blanco-Rodriguez, A. M.; Záliš, S.; Vlček, A., Jr.; Tavernelli, I.; Rothlisberger, U.; Milne, C. J.; Chergui, M. X-ray absorption spectroscopy of ground and excited of rhenium-carbonyl-diimine complexes: evidence for a two-center electron Transfer. *J. Phys. Chem. A* **2013**, *117*, 361−369.
(46) Gourlaouen, C.; Eng, J.; Otsuka, M.; Gindensperger, E.; Daniel, C. A quantum chemical interpretation of ultra-fast luminescence decay and intersystem crossings in Rhenium (I) carbonyl bipyridine complexes. *J. Chem. Theory Comput.* **2015**, *11*, 99−110 DOI: 10.1021/ct500846n.
(47) J. Tomasi, J.; Persico, M. Molecular interactions in solution: An overview of methods based on continuous distributions of the solvent. *Chem. Rev.* **1994**, *94*, 2027−2094.
(48) Tomasi, J.; Mennucci, B.; Cammi, R. Quantum mechanical continuum solvation models. *Chem. Rev.* **2005**, *105*, 2999−3093.
(49) Stephens, P. J.; Devlin, F. J.; Chabalowski, C. F.; Frisch, M. J. *Ab initio* calculation of vibrational absorption and circular dichroism spectra using density functional force fields. *J. Phys. Chem.* **1994**, *98*, 11623−11627.
(50) van Lenthe, E.; Baerends, E. J. Optimized Slater-type basis sets for the elements 1−118. *J. Comput. Chem.* **2003**, *24*, 1142−1156.
(51) van Lenthe, E.; van Leeuwen, R.; Baerends, E. J.; Snijders, J. G. Relativistic regular two-component Hamiltonians. *Int. J. Quantum Chem.* **1996**, *57*, 281−293.
(52) Wang, F.; Ziegler, T. A simplified relativistic time-dependent density-functional theory formalism for the calculations of excitation energies including spin-orbit coupling effect. *J. Chem. Phys.* **2005**, *123*, No. 154102.
(53) Meyer, D.-H.; Manthe, U.; Cederbaum, L. S. The multi-configurational time-dependent Hartree approach. *Chem. Phys. Lett.* **1990**, *165*, 73−78.
(54) Beck, M. H.; Jäckle, A.; Worth, G. A.; Meyer, H.-D. The multiconfiguration time-dependent Hartree (MCTDH) method: a highly efficient algorithm for propagating wavepackets. *Phys. Rep.* **2000**, *324*, 1−105.
(55) Meyer, H.-D., Gatti, F., Worth, G. A., Eds. *Multidimensional Quantum Dynamics: MCTDH Theory and Applications*; Wiley-VCH: Weinheim, Germany, 2009.
(56) Worth, G. A.; Beck, M. H.; Jäckle, A.; Meyer, H.-D. The MCTDH Package, version 8.2, University of Heidelberg, Heidelberg, Germany, 2000. Meyer, H.-D. The MCTDH Package, version 8.3, University of Heidelberg, Heidelberg, Germany, 2002, Meyer, H.-D. The MCTDH Package, version 8.4, University of Heidelberg, Heidelberg, Germany, 2007. Vendrell, O.; Meyer, H.-D. The MCTDH Package, version 8.5, University of Heidelberg, Heidelberg, Germany, 2011. See http://mctdh.uni-hd.de.

DOI: 10.1021/ar500369r
Acc. Chem. Res. 2015, 48, 809−817